PASJ: Publ. Astron. Soc. Japan , 1–??, published

Suzaku Spectroscopy of an X-Ray Reflection Nebula and a New Supernova Remnant Candidate in the Sgr B1 Region

Masayoshi NOBUKAWA, Takeshi Go TSURU, Yojiro TAKIKAWA, Yoshiaki HYODO, Tatsuya INUI,
Hiroshi NAKAJIMA, Hironori MATSUMOTO and Katsuji KOYAMA,
Department of Physics, Graduate School of Science, Kyoto University, Sakyo-ku, Kyoto 606-8502
nobukawa@cr.scphys.kyoto-u.ac.jp
Hiroshi MURAKAMI
PLAIN center, ISAS/JAXA, 3-1-1 Yoshinodai, Sagamihara, Kanagawa 229-8510
and
Shigeo YAMAUCHI
Faculty of Humanities and Social Sciences, Iwate University, 3-18-34 Ueda, Morioka, Iwate 020-8550

(Received 2007 May 4; accepted 2007 August 27)

Abstract

We made a 100 ks observation of the Sagittarius (Sgr) B1 region at $(l,\ b) = (0.^\circ5,\ -0.^\circ1)$ near to the Galactic center (GC) with the Suzaku/XIS. Emission lines of S XV, Fe I , Fe XXV, and Fe XXVI were clearly detected in the spectrum. We found that the Fe XXV and Fe XXVI line emissions smoothly distribute over the Sgr B1 and B2 regions connecting from the GC. This result suggests that the GC hot plasma extends at least up to the Sgr B region with a constant temperature. There are two diffuse X-ray sources in the observed region. One of the two (G0.42−0.04) is newly discovered, and exhibits a strong S XV Kα emission line, suggesting a candidate for a supernova remnant located in the GC region. The other one (M0.51−0.10), having a prominent Fe I Kα emission line and a strongly absorbed continuum, is likely to be an X-ray reflection nebula. There is no near source bright enough to irradiate M0.51−0.10. However, the Fe I Kα emission can be explained if Sgr A* was $\sim 10^6$ times brighter 300 years ago, the light travel time for 100 pc to M0.51−0.10, than it is at present.

Key words: ISM: clouds—ISM: supernova remnants—X-rays: ISM

1. Introduction

One of the remarkable discoveries from X-ray observations of the Galactic center (GC) region is the Galactic center diffuse X-ray emission (GCDX) extending over ∼300 pc ($|l| < 1^\circ$), and that the GCDX has a prominent highly ionized iron line at 6.7 keV (Koyama et al. 1989; Yamauchi et al. 1990). ASCA detected Fe XXV and Fe XXVI emission lines from the GCDX, and its spectrum could interpreted to be emitted from a hot plasma of $kT \sim 10$ keV (Koyama et al. 1996). Chandra, with an extremely high spatial resolution of $\sim 0.''5$, has detected many X-ray point sources in the GC region. The total flux of the detected point sources is not enough to explain all of the GCDX (Muno et al. 2004). On the other hand, Revnivtsev et al. (2006) indicate that the X-ray emission can be completely explained by integration of point sources. Suzaku revealed that the origin of the iron lines is not the charge-exchange of cosmic-rays with molecular clouds, but collisional ionization of hot plasma with a temperature of $kT \sim 6.5$ keV (Koyama et al. 2007c). Moreover, the spatial distribution is different from that of point sources observed by Chandra, suggesting that the main part of the emission is from truly diffuse plasma in $l = -0.^\circ4 - +0.^\circ2$ (Koyama et al. 2007c). Where the hot plasma has extended is not yet clear.

In addition, the origin of the huge thermal energy (10^{53-54} ergs) of the hot diffuse plasma is a serious mystery. One hypothesis is a multiple supernova explosions scenario in which the dynamical timescale of 10^5 years for the hot plasma requires tens of supernova explosions during a period of ten thousand years. Since a few supernova remnants (SNRs) have been detected so far, there would exist many undiscovered SNRs.

Another remarkable discovery is diffuse emission of Fe I at 6.4 keV. It was firstly detected by ASCA. In particular, bright emission regions of the 6.4 keV line have consistent positions of the giant molecular clouds of Sgr B2, Sgr C, and the Radio Arc (Koyama et al. 1996; Murakami et al. 2001a; Murakami et al. 2001b). Their X-ray spectra exhibit a large equivalent width ($\gtrsim 1$ keV) for the Fe I emission line and deep absorption column ($\gtrsim 10^{23}$ cm^{-2}). This suggests that those molecular clouds were irradiated with hard X-rays from an external source and "reflected" them as the 6.4 keV X-rays (X-ray reflection Nebulae; XRNe). There is no irradiating source with a luminosity of $\gtrsim 10^{39}$ ergs s^{-1} to explain those 6.4 keV X-rays in the GC region. Koyama et al. (1996) proposed a scenario of a past X-ray outburst of the supermassive black hole at Sgr A*. Since its present luminosity is 2×10^{33} ergs s^{-1} (Baganoff et al. 2003), it would have been 10^6 times brighter than now 300 years ago.

On the other hand, Yusef-Zadeh et al. (2007) suggest that the 6.4 keV X-rays are due to collision of low-energy

cosmic-ray electrons with this molecular gas because of a correlation between non-thermal radio filaments and the X-ray features. The scenario explains not only the Fe I Kα emission, but also the cosmic-ray heating of molecular gas and diffuse TeV emission from the Galactic molecular clouds.

The radio complex Sgr B1, located to the west, or to the negative Galactic longitude of the Sgr B2 giant molecular cloud consists of a H II region surrounded by a molecular loop (Sofue 1990). The expansion of the molecular loop is explained by past activity of the H II region (Sofue 1990). A 6.4 keV clump was discovered in this region by Yusef-Zadeh et al. (2007). OH and H_2O masers have been found, and many intermediate and/or low-mass stars are formed (Mehringer et al. 1993).

The X-ray Imaging Spectrometers (XIS) aboard Suzaku have characteristic features of a large effective area and a low/stable background. The XIS are instruments suitable to observe diffuse and faint objects, such as XRNe and SNRs. We had observed the Sgr B1 region for about 100 ksec with Suzaku in order to obtain a good spectrum of the new 6.4 keV cloud detected by Yusef-Zadeh et al. (2007). We report on results of the observation.

2. Observation and Data Processing

We observed the Sgr B1 region with Suzaku on 2006 March 27–29. Though the Suzaku observation was performed with the Hard X-ray Detector (Takahashi et al. 2007; Kokubun et al. 2007) and the XIS, we concentrate on the XIS data in this paper. The XIS system consists of four sets of CCD cameras (designated as XIS0, 1, 2, and 3) placed on the focal planes of the four X-Ray Telescopes (XRT), whose half-power diameters are $\sim 2'$ (Serlemitsos et al. 2007). XIS0, 2, and 3 have front-illuminated (FI) CCDs, while XIS1 contains a backside-illuminated (BI) CCD. The energy resolution of the XIS was ~ 170 eV at 5.9 keV (calibration source of ^{55}Fe) when this observation was performed. The details of Suzaku, XIS, and XRT are given in Mitsuda et al. (2007), Koyama et al. (2007a), and Serlemitsos et al. (2007), respectively.

The XIS data were taken in the normal mode. The XIS pulse-height data for each X-ray event were converted to Pulse Invariant (PI) channels using the xispi software version 2006-12-26, and the calibration database version 2006-05-22. After removing the epoch of low-Earth elevation angles less than 5 degrees (ELV$< 5^\circ$), the day Earth elevation angle less than 10 degrees (DYE_ELV$< 10^\circ$) and the South Atlantic Anomaly (SAA), the effective exposure time was about 95 ks. We performed the data reduction and the analysis using HEADAS software 6.1.2 and `XSPEC` 11.3.2. In spectral fittings, we used the XIS response files released on 2006-08-01 by the Suzaku XIS team, and generated auxiliary files with `xissimarfgen` in HEADAS software 6.1.2. Since the relative gains among FI sensors are well calibrated and the response functions are essentially the same, we co-added their data. We also applied non-X-ray background (NXBG) data from the night-Earth data released by the Suzaku XIS team.[1] The NXBG data were sorted with the geomagnetic cut-off rigidity (COR) because of the variation of the NXBG corresponding to the COR values.

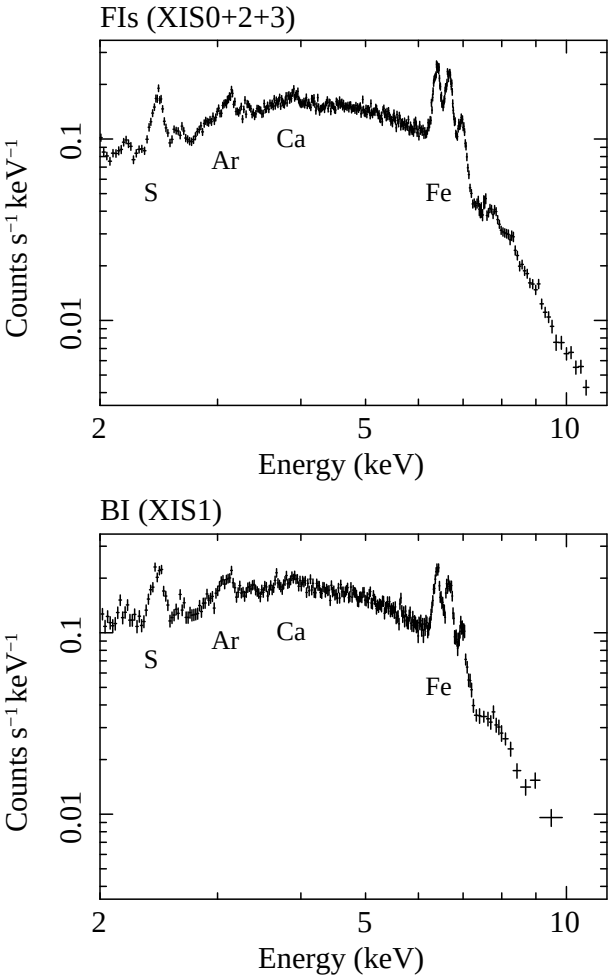

Fig. 1. Suzaku/XIS spectra of the Sgr B1 region. The top and bottom panels show the co-added spectrum of the FIs (XIS0+2+3) and that of the BI (XIS1), respectively. The spectra were collected from the full FOV, but excluded the corners where the calibration sources (^{55}Fe) illuminate the Mn I K lines. The non-X-ray backgrounds were already subtracted.

3. Analysis and Results

3.1. The Overall Features

We show the X-ray spectra of the Sgr B1 region in figure 1. They are the FI (the average of XIS0, 2, and 3; top) and BI (XIS1; bottom) spectra extracted from the full FOV, excluding the corners where the calibration sources of ^{55}Fe illuminate. The NXBG was already subtracted from the spectra. They show K emission lines from He-like and/or H-like ions of S, Ar, Ca, and Fe. In addition, the Kα emission line at 6.4 keV and the K-edge absorption at 7.1 keV of neutral or low ionized Fe are clearly

[1] http://www.astro.isas.jaxa.jp/suzaku/analysis/xis/nte/

detected. Three Fe lines at 6.4, 6.7, and 6.9 keV are well resolved, thanks to the excellent energy resolution of the XIS.

We examined the characteristic lines of Fe I, Fe XXV, Fe XXVI, and S XV. We show narrow-band images of 2.45 keV (2.35–2.55 keV; S XV), 6.4 keV (6.30–6.50 keV; Fe I), and 6.7 keV (6.57–6.77 keV; Fe XXV) in figure 2a, 2b and 2c, respectively. They are co-added images of the four XIS, in which the NXBG was subtracted and the correction of exposure and vignetting effects had already been done. The exposure maps were made with `xissim` (Ishisaki et al. 2007) in HEADAS software 6.1.2.

We can see two clear diffuse sources in the two elliptic solid regions shown in figures 2a and 2b. We hereafter call the source in figure 2(a) "Suzaku J1746.4−2835.4 (G0.42−0.04)" and that in figure 2(b) "Suzaku J1747.1−2833.2 (M0.51−0.10)", respectively. G0.42−0.04 is a newly discovered source in this observation. M0.51−0.10 is identified with the 6.4 keV cloud "Sgr B1", discovered by Yusef-Zadeh et al. (2007), whose position of $(l,\ b) \sim (0.^\circ5,\ -0.^\circ1)$ is the same.

We here note excesses near the western edge of the FOV in each image. A known bright X-ray source with a flux of a few 10^{-10} ergs s^{-1} cm^{-2}, 1E 1743.1−2843, is located outside the FOV in the northwest direction (Del Santo et al. 2006), and its position is marked with a small green circle in figure 2. The northwest excess is due to the XRT PSF (point spread function) tail of 1E 1743.1−2843. It has a hard X-ray spectrum, which is consistent with the result that the northwest excess is seen in all panels in figure 2.

The southwest excess is seen only in figure 2a. Dutra and Bica (2000) reported that two stellar clusters (DB00–5 and DB00–6) are located at the position marked in figure 2a. Law and Yusef-Zadeh (2004) identified them as soft X-ray sources with the fluxes of $10^{-14}-10^{-13}$ ergs s^{-1} cm^{-2} in the 2 to 10 keV band, and suggested that the stellar clusters are located in the foreground of the GC region. The preliminary analyses of our observation show that the southeast excess in figure 2a have consistent flux with those reported for the stellar clusters.

3.2. Spatial Distribution of the Fe XXV Kα Emission

Figure 2c and figure 3 show a narrow-band image of 6.7 keV (Fe XXV), namely the distribution of the GCDX. Figures 4, 5, and 6 of Koyama et al. (2007c) give profiles of the fluxes of the 6.7 keV line and the flux ratios of 6.7 and 6.9 (Fe XXVI) keV lines as a function of the galactic longitude between $l = -0.^\circ4 - +0.^\circ2$. We made the same profiles for the Sgr B1 region of $l = +0.^\circ3 - +0.^\circ6$, and compared them with the results of Koyama et al. (2007c).

First, we divided the Sgr B1 region into 4 × 4 small regions, excluding the four corners illuminated by the built-in calibration sources, as shown in figure 2d. Next, we obtained the co-added spectrum of the 3 FIs (XIS0, 2, and 3) for each small region. We finally obtained 6.7 keV and 6.9 keV line fluxes and their ratio for each small region by fitting the spectrum with a continuum (thermal bremsstrahlung), Fe lines, which are Fe I Kα and Kβ (6.4 and 7.05 keV), Fe XXV Kα (6.7 keV), and Fe XXVI Lyα (6.9 keV), and the cosmic X-ray background (CXB). Koyama et al. (2006) suggested that the 6.7 keV emission smoothly extends to the Sgr B2 region ($l = +0.^\circ6 - +0.^\circ8$) with almost the same temperature. Thus, we made follow-up analyses on the Fe emission lines for the Sgr B2 region by the same method as was used for Sgr B1.

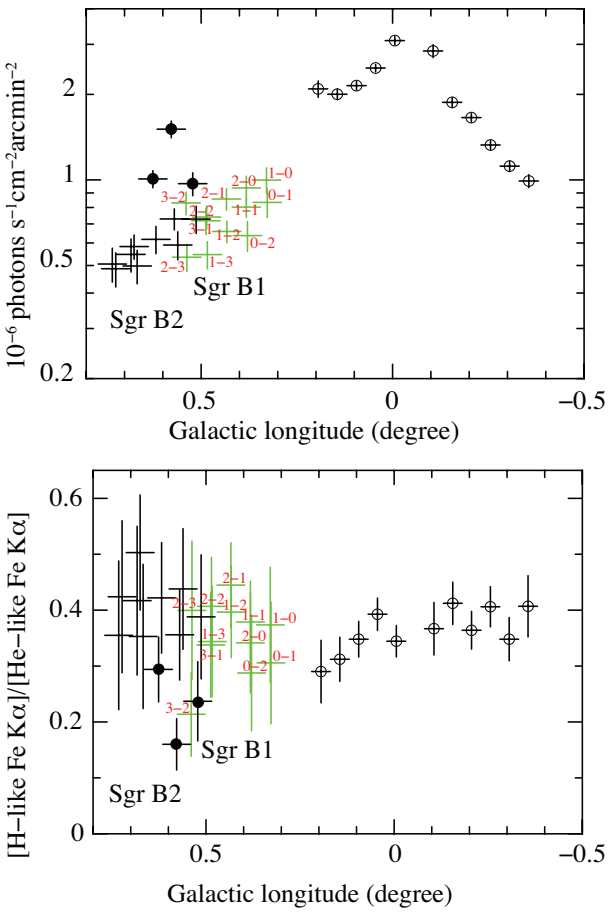

Fig. 4. Top panel: The 6.7 keV line fluxes of the GC region at $l = -0.^\circ4 - +0.^\circ8$, including the Sgr B1 and B2 regions. The data of the Sgr B1 region obtained in this observation are colored with green. Data marked with open circles are adopted from Koyama et al. (2007c). The data with filled circles correspond to SNR G0.61+0.01 (Koyama et al. 2007b). The ID number of the data correspond to the regions with the same ID number as in figure 2d. Bottom panel: The same as in the top panel, but for the photon flux ratios between the 6.7 and 6.9 keV lines.

In figure 4, we show the 6.7 keV line flux (top) and the ratio between the photon fluxes of the 6.7 keV and 6.9 keV lines (bottom) as a function of the Galactic longitude. Excluding the data of the region at G0.61+0.01 (will be mentioned later on), we found that the 6.7 keV line flux exponentially decreases from the peak at the GC ($l \sim -0.^\circ05$), and smoothly connects the Sgr B1 and B2 regions. The line-flux ratios of [Fe XXVI]/[Fe XXV] in the Sgr B1 and B2 regions are almost the same as those in $l = -0.^\circ4 - +0.^\circ2$.

We note that the three data points indicated with filled

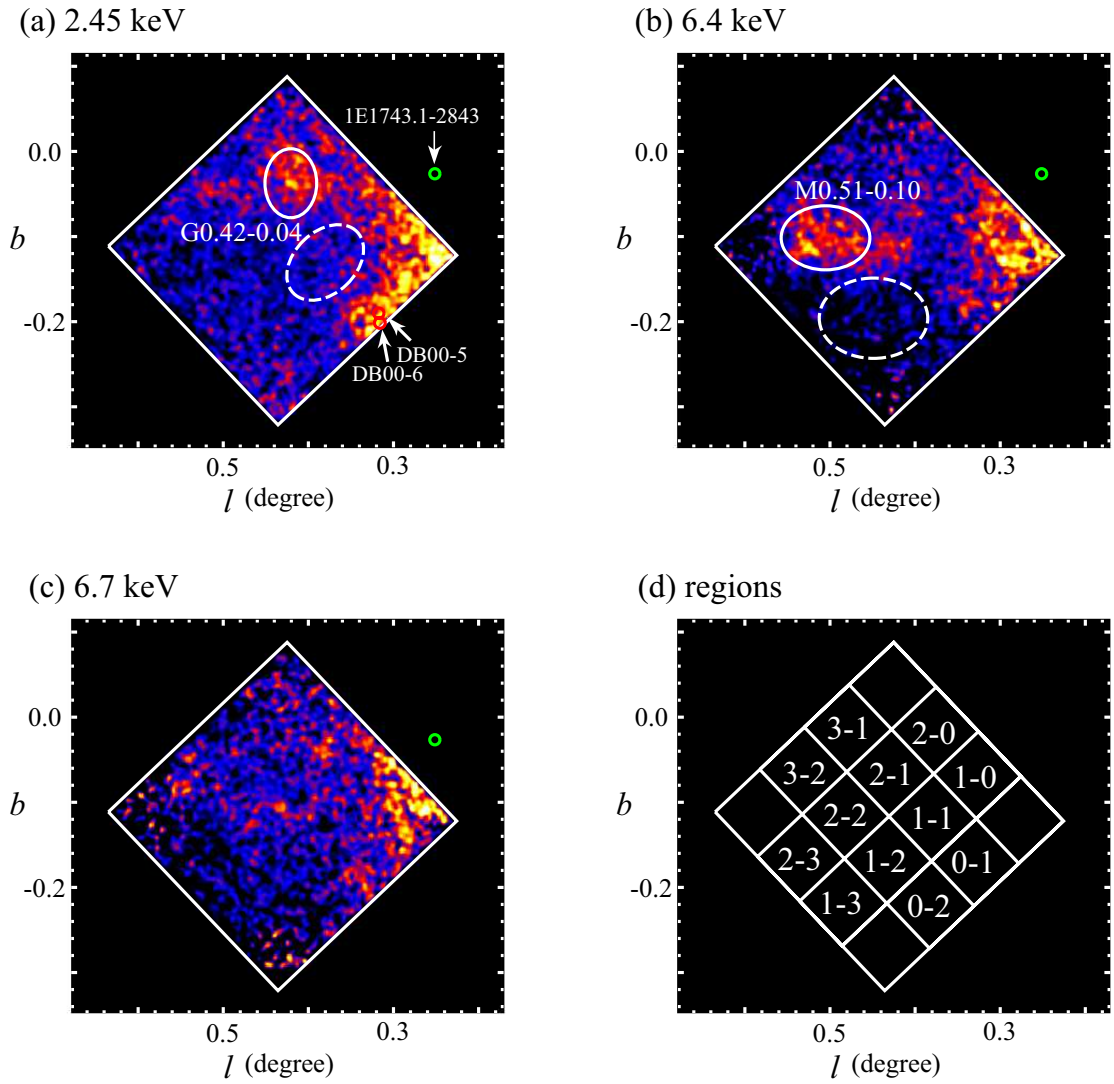

Fig. 2. Narrow-band images in the 2.35–2.55 keV (a), 6.30–6.50 keV (b), and 6.57–6.77 keV (c). They are the co-added images of the four XIS. Subtraction of the NXBG had already been done, and the effects of exposure and vignetting were taken into account. We collected spectra of G0.42−0.04 and its background from the solid and dashed line regions in panel (a), respectively. The solid and dashed lines in panel (b) show the regions for the spectra of M0.51−0.10 and its background, respectively. The minor and major axes of each elliptical region are $1\farcm8 \times 2\farcm4$ (G0.42−0.04: source), $2\farcm2 \times 3\farcm1$ (G0.42−0.04: background), $2\farcm3 \times 3\farcm1$ (M0.51−0.10: source), $2\farcm8 \times 3\farcm8$ (M0.51−0.10: background), respectively. (d) shows the small square regions and their ID numbers used in sec 3.2

circles in the Sgr B2 region, having high 6.7 keV fluxes and low flux ratios between the 6.7 keV and 6.9 keV lines, correspond to SNR G0.61+0.01, which Koyama et al. (2007b) recently discovered with Suzaku. The plasma temperature of G0.61+0.01 is $kT \sim 3$ keV (Koyama et al. 2007b), which is significantly lower than that of the GCDX ($kT \sim$6–7 keV: Koyama et al. 2007c). We can see that the 6.7 keV intensity of the small region [3–2] is rather higher than expected from the whole tendency, and that the ratio of [Fe XXVI]/[Fe XXV] is lower than the average of the GCDX. G0.61+0.01 is located to the east of the small region [3–2] (see figure 3). This result suggests that the SNR would have a larger size than the one reported by Koyama et al. (2007b), and that the small region [3–2] is a part of G0.61+0.01.

3.3. Discovery of a 2.45 keV Clump, G0.42−0.04

The background-subtracted spectra of the new source, G0.42−0.04, are shown in figure 5. We ignored the energy range at the Si absorption edge due to the CCDs used in the XIS, where the systematic uncertainties still remained in the response matrices available at the time of writing this paper. The background for G0.42−0.04 consists of the NXBG, CXB, and GCDX. As shown in the previous section, the X-ray flux from the GCDX is rather different from position to position. We thus selected the dashed region in figure 2a for the background region, so that the average line flux of the 6.7 keV line

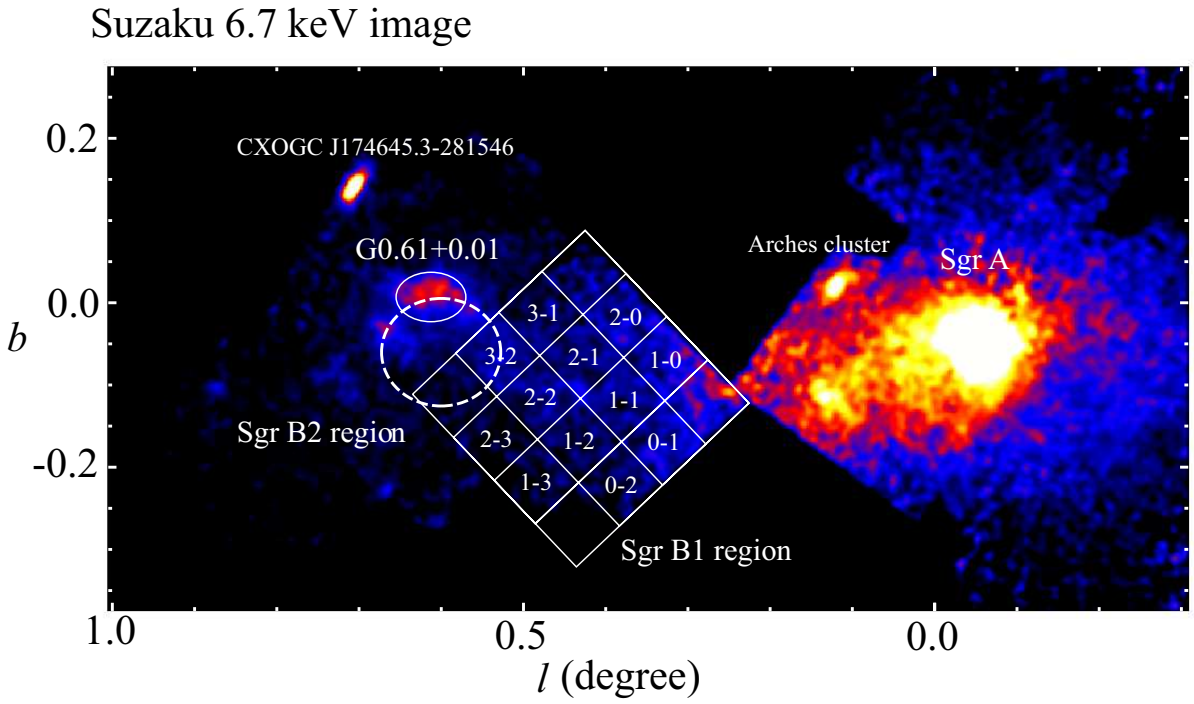

Fig. 3. The 6.7 keV band image of the Sgr A to Sgr B2 regions with Suzaku. Excepting Sgr B1, the image is adopted from Koyama et al. (2007b), Koyama et al. (2007c), Hyodo et al. (2008) and Mori et al. (2008). The small square regions and the numbers are the same as in figure 2d. G0.61+0.01 is located to the east of the Sgr B1 region (the solid ellipse; Koyama et al. 2007b). We can think that G0.61+0.01 is a part of the dashed shell. There are other bright sources: CXOGC J174645.3–281546 (Muno et al. 2006; Hyodo et al. 2008) and Arches cluster (Tsujimoto et al. 2007).

(the reference of the GCDX) is almost the same between the region for the G0.42−0.04 (the small region [2–1]) and the one for the background (the small regions [1–0] and [1–1]). Figure 5 shows no residuals at the iron emission lines of 6.7 and 6.9 keV. It is thus confirmed that background emission from the GCDX was successfully subtracted. Additionally, the NXBG and CXB are also thought to be subtracted.

Since there exist many X-ray point sources in the GC region, we next checked the contribution from point sources. According to the X-ray point-source catalog with Chandra (Muno et al. 2006), the fluxes per square arcminute (2–8 keV) from point sources are 9.9×10^{-15} ergs cm^{-2} s^{-1} arcmin^{-2} (8 point sources) in the region of G0.42−0.04, and 7.8×10^{-15} ergs cm^{-2} s^{-1} arcmin^{-2} (10 sources) in the background region, respectively. The difference of 2.1×10^{-15} ergs cm^{-2} s^{-1} arcmin^{-2} corresponds to 20% of the surface brightness of G0.42−0.04, itself (1.2×10^{-14} ergs cm^{-2} s^{-1} arcmin^{-2}), observed by Suzaku.

Pronounced features of the spectra are the S XV line (2.45 keV), a cut-off below 2 keV, and a steep slope above 4 keV. We fitted the spectra with a simple model of an absorbed thin thermal plasma (`VAPEC` model in `XSPEC`) for G0.42−0.04 plus a model of an absorbed power-law component representing the residual spectrum of the point sources. We fixed the model parameters for the power-law component to be those given in table 1 while referring to Muno et al. (2006). The spectra were nicely fitted with a model with a plasma temperature of ~ 0.7 keV. The absorption column of $\sim 8 \times 10^{22}$ cm^{-2} is consistent with a source in the GC region (6×10^{22} cm^{-2}), which suggests that G0.42−0.04 is located in the GC region. Assuming a distance of 8.5 kpc and the shape of G0.42−0.04 to be like a rugby ball, its 3-axis radii are 6 pc × 4.5 pc × 4.5 pc.

3.4. Spectrum of a 6.4 keV Clump, M0.51−0.10

We examined M0.51−0.10, a diffuse source in the 6.4 keV narrow-band image of figure 2b. We identified this diffuse source with the 6.4 keV cloud "Sgr B1" detected by Yusef-Zadeh et al. (2007). However, we call the 6.4 keV cloud "M0.51−0.10" in order to avoid any confusion with the H II region "Sgr B1" at $(l, b) = (0.^\circ5, -0.^\circ05)$ near the 6.4 keV cloud.

We obtained the background-subtracted spectra shown in figure 6, in which the source and the background-spectra were extracted from the solid and dashed regions in figure 2b, respectively. Because we selected the background region while referring to the top panel of figure 4, the 6.7 keV line fluxes, namely the GCDX, of the two regions are almost the same level within the statistical errors. We assume that since the NXBG and CXB are the same in the source and background regions, their contri-

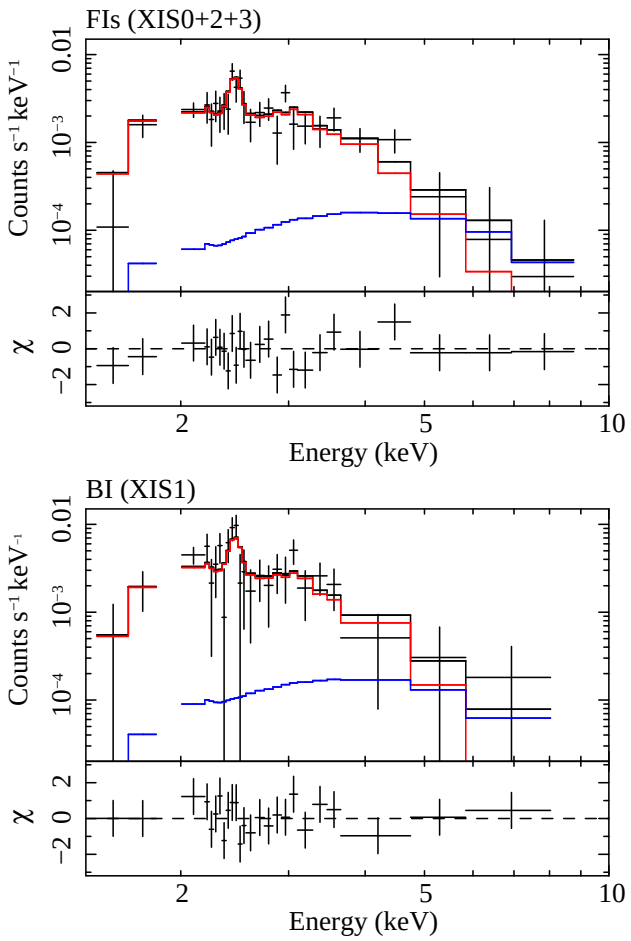

Fig. 5. Background-subtracted FIs (top) and BI (bottom) spectra of G0.42−0.04. The source and background data were extracted from the solid and dashed regions in figure 2a, respectively. The red and blue model lines show the plasma component and the residual of the point sources, respectively.

butions were successfully subtracted.

We checked a residual contribution of point sources after the background subtraction with the point-source catalog by Muno et al. (2006). There are 14 and 11 point sources in the source and background regions, respectively. Those fluxes per square arcminute in the 2 to 10 keV band are 5.0×10^{-15} ergs cm^{-2} s^{-1} arcmin^{-2} in the source region, and 6.4×10^{-15} ergs cm^{-2} s^{-1} arcmin^{-2} in the background region. Though the flux in the background region is somehow larger than that in the source region, the difference (1.4×10^{-15} ergs cm^{-2} s^{-1} arcmin^{-2}) is only 3% of the flux of M0.51−0.10 (5.4×10^{-14} ergs cm^{-2} s^{-1} arcmin^{-2}). Thus, the contribution from the point sources after background subtraction can be ignored.

The XIS spectra of M0.51−0.10 contain a prominent 6.4 keV emission line. We fitted the spectra with a model consisting of an absorbed power-law component plus two Gaussian lines of Fe I Kα (6.4 keV) and Kβ (7.06 keV). We obtained an acceptable result, and give the best-fit parameters in table 2. Yusef-Zadeh et al. (2007) reported that the equivalent width of the Fe I Kα line is $\sim$0.6 keV, smaller than our results of $\sim$1.4 keV. Yusef-Zadeh et al. (2007) subtracted only the NXBG from the source spectrum. We examined that the equivalent width of the Fe I Kα line was obtained to be $\sim$0.5 keV from our spectra when we subtracted only the NXBG from the source spectra. We believe that the difference between the result of Yusef-Zadeh et al. (2007) and ours is due to different assumptions concerning the background emission.

Table 1. Result of a spectral fitting of G0.42−0.04 with `VAPEC` in `XSPEC`.

Model component	Value
Absorption1 ($N_{\rm H}$) (10^{22} cm^{-2})	$7.9^{+1.1}_{-1.5}$
CIE Plasma (VAPEC):	
Temperature kT (keV)	$0.70^{+0.23}_{-0.21}$
Abundance Sulfur (solar)	$0.9^{+0.4}_{-0.3}$
Normalization*	$8.8^{+0.8}_{-0.9}$
(Residual point source component)§	
Absorption2 ($N_{\rm H}$) (10^{22} cm^{-2})	6.0
Power-law:	
Photon index Γ	1.5
Normalization‖	1.0
Observed Flux (10^{-13} ergs cm^{-2} s^{-1})†	$1.4^{+0.2}_{-0.1}$
Luminosity (10^{33} ergs s^{-1})‡	$6.5^{+0.5}_{-0.6}$
χ^2/dof	33/48

The uncertainties indicate the 90% confidence levels.
* $10^{-11}/(4\pi D^2)\int n_{\rm e} n_{\rm H} dV$, where D is the distance to the source (cm), $n_{\rm e}$ and $n_{\rm H}$ are the electron and hydrogen density (cm^{-3}), respectively.
§ The shape of the spectrum is referred to Muno et al. (2006). These parameters are fixed.
‖ The unit is 10^{-5} photons cm^{-2} s^{-1} keV^{-1} at 1 keV.
† In the 2 to 8 keV band, except the residual point source component.
‡ Absorption corrected in the 2 to 8 keV band, except the residual point source component. The distance toward G0.42−0.04 is assumed to be 8.5 kpc.

4. Discussion

4.1. The Thermal Plasma Clump, G0.42-0.04

We here discuss the nature of G0.42−0.04 as an SNR. Assuming an uniform plasma filling the rugby ball region, we obtained the physical parameters of G0.42−0.04 given in table 3. The plasma temperature of $kT \sim 0.7$ keV and the size of $\sim$10 pc are typical values for an SNR. On the other hand, the thermal energy of 4×10^{49} ergs is lower than the canonical value of $0.7 \times E_{\rm total} \sim 0.7 \times 10^{51}$ ergs for an ordinary SNR in the Sedov phase. The dynamical timescale can be obtained to be $\sim$8000 years from the sound velocity of 7×10^7 cm s^{-1} for a plasma with $kT \sim 0.7$ keV and the size of G0.42−0.04. Assuming the timescale as the age of an SNR, the size of $\sim$10 pc and the total mass of 12 $M_\odot$ for G0.42−0.04 are smaller than the values of $\sim$20 pc and $\sim$100 $M_\odot$ for a typical SNR having a similar age in the Sedov phase. A general structure of an SNR is that the temperature of the center is higher than that in the shell, while the surface brightness in the center is much lower than that in the shell. Thus, it is possible that the soft X-ray emission from the shell of G0.42−0.04

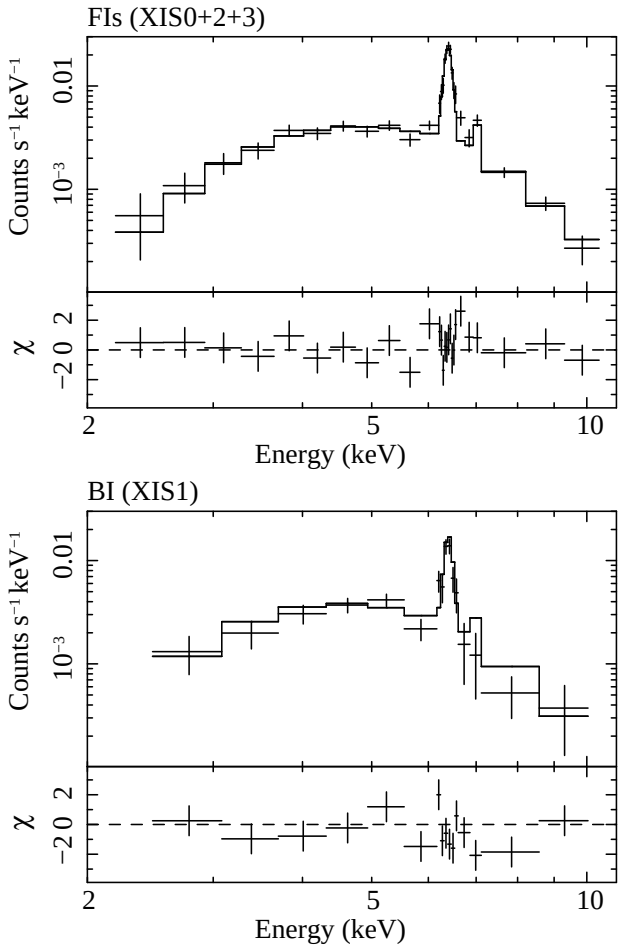

Fig. 6. The M0.51−0.10 spectra of the FIs (top) and BI (bottom). The source and background spectra were extracted from the solid and dashed region in figure 2(b), respectively.

would be absorbed by the large absorption column toward the GC. Thus, the results of our observation are consistent with an SNR. We conclude that G0.42−0.04 is an SNR candidate.

We examine another possibility, that G0.42−0.04 is a stellar cluster. The temperature of $kT \sim 0.7$ keV is in the range of the typical value of $0.5 \sim 3$ keV for a stellar cluster. The X-ray luminosity, 6×10^{33} ergs s^{-1}, of G0.42−0.04 is similar to 2×10^{34} ergs s^{-1} for the Arches cluster (Tsujimoto et al. 2007) and 1×10^{34} ergs s^{-1} for the Quintuplet cluster (Law and Yusef-Zadeh 2004), both of which are famous stellar clusters in the GC region. The absorption column toward G0.42–0.04 ($\sim 8 \times 10^{22}$ cm^{-2}) is rather less than that toward the Arches cluster ($\sim 14 \times 10^{22}$ cm^{-2}; Tsujimoto et al. 2007). Dutra and Bica (2000) searched for stellar clusters in a field of $5^\circ \times 5^\circ$, centred close to the Galactic Nucleus using the infrared 2MASS Survey archive. In their catalog, no cluster is reported for the position of G0.42−0.04. Thus, it is unlikely that G0.42−0.04 is a stellar cluster.

Table 2. Result of a spectral fitting of the M0.51−0.10. The model is an absorbed power-law plus two Gaussian lines.

Model component	Value
Absorption ($N_{\rm H}$) (10^{23} cm^{-2})	$1.5^{+0.2}_{-0.1}$
Continuum (power-law):	
Photon index (Γ)	$1.8^{+0.4}_{-0.5}$
Gaussian1 (Fe I Kα):	
Line center energy (eV)	6402^{+6}_{-7}
Intensity (10^{-5} photons cm^{-2} s^{-1})	$2.8^{+0.2}_{-0.4}$
Equivalent Width (keV)	$1.4^{+0.3}_{-0.3}$
Gaussian2 (Fe I Kβ):	
Line center energy (eV)*	7061
Intensity (10^{-5} photons cm^{-2} s^{-1})	$0.44^{+0.17}_{-0.21}$
Equivalent Width (keV)	$0.23^{+0.22}_{-0.21}$
Observed Flux (10^{-12} ergs cm^{-2} s^{-1})†	$1.2^{+0.1}_{-0.1}$
Luminosity (10^{34} ergs s^{-1})‡	$1.9^{+0.1}_{-0.1}$
χ^2/dof	50/37

The uncertainties indicate the 90% confidence limits.
* Fixed to $1.103 \times E$(Fe I Kα).
† In the 2 to 10 keV band.
‡ Absorption corrected in the 2 to 10 keV band.

Table 3. Physical parameters of G0.42−0.04.

Parameter	Value
EM* (cm^{-3})	8×10^{57}
$n_{\rm e}$† (cm^{-3})	0.8
M‡ ($M_\odot$)	12
$E_{\rm thermal}$§ (ergs)	4×10^{49}
$t_{\rm dyn}$‖ (year)	8000

The plasma is assumed to be uniform density and elliptical shape with 3-axis radii of 6 pc × 4.5 pc × 4.5 pc.
* The emission measure (EM) $= n_{\rm e} n_{\rm H} V$, where $n_{\rm e}$ and $n_{\rm H}$ are the electron and hydrogen densities and assumed to be equal. V is the plasma volume.
† The electron density.
‡ The total mass $= n_{\rm e} m_{\rm p} V$, where $m_{\rm p}$ is the proton mass.
§ The thermal energy $E_{\rm thermal} = 3 n_{\rm e} k T V$.
‖ The dynamical time scale. The sound velocity of the ~ 0.7 keV plasma is 7×10^7 cm s^{-1}.

4.2. The 6.4 keV Clump, M0.51–0.10

The absorption column of 1.5×10^{23} cm^{-2} is 2-times or more larger than the typical value of 6×10^{22} cm^{-2} for sources in the GC region. The strong 6.4 keV emission line implies that a large amount of iron in the neutral state exists at M0.51−0.10. Thus, these results suggest M0.51−0.10 is a local cool dense cloud in the GC region. Indeed, a molecular cloud lies at the same position of M0.51−0.10, which is a part of the Sgr B1 molecular shell proposed by Sofue (1990).

Two possible scenarios for the the origin of the 6.4 keV emission line have been proposed. One is photo-ionization by X-rays, namely the XRN scenario. The other is inner-shell ionization by the collision of low-energy cosmic-ray electrons. The observed large equivalent width of 1.4 keV

and an absorption column reaching $\sim 10^{23}$ cm^{-2} are consistent with those of the XRN scenario. On the other hand, the scenario of electron collision expects a rather small equivalent width of ~ 300 eV and an absorption column of less than $\sim 10^{21-22}$ cm^{-2}, assuming that the elemental composition is the same as that of the solar system (Tatischeff 2003). The electron-collision scenario requires an iron over-abundance by a factor of 4 – 5, while the photo-ionization model does not require an iron over-abundance. Thus, we conclude that M0.51−0.10 is likely to be an X-ray reflection nebula.

4.3. X-Ray Source Irradiating M0.51− 0.10

In order to examine the irradiating source, we estimate its luminosity to require the M0.51−0.10 fluorescence. The XRN absorbs X-rays with energies higher than 7.1 keV from the external source, and emits a fluorescent line of 6.4 keV X-rays. The photon flux of the 6.4 keV line, $C_{6.4\mathrm{keV}}$ (photons s^{-1} cm^{-2}), is described by the following equation:

$$C_{6.4\mathrm{keV}} = \epsilon \frac{\Omega}{4\pi} \int_{7.1\mathrm{keV}}^{\infty} \left(1 - e^{-N_{\mathrm{Fe}}\sigma_{\mathrm{Fe}(E)}}\right) AE^{-\Gamma} dE. \quad (1)$$

Here, we assume that the irradiating source has a power-law spectrum ($AE^{-\Gamma}$) and the iron abundance of the molecular cloud of M0.51−0.10 is solar ([Fe]/[H] = 3×10^{-5}). Since the typical absorption column for sources in the GC region is $N_{\mathrm{H}} = 0.6 \times 10^{23}$ cm^{-2}, that of M0.51−0.10, itself, is estimated to be $N_{\mathrm{H}} = 0.9 \times 10^{23}$ cm^{-2} from the results of the spectral fitting. $\Omega = \pi(r/D)^2$ is the solid angle covered by M0.51−0.10 from the view point of the irradiating source, where r is the radius of M0.51−0.10 and D is the distance between M0.51−0.10 and the irradiating source; ϵ is a fluorescent yield of 0.34 for iron atom. The K-shell photo-ionization cross section per an iron atom against an X-ray with energy above 7.1 keV is $\sigma_{\mathrm{Fe}} = 6.0 \times 10^{-18}(E/1\mathrm{keV})^{-2.58}$ (cm^2) (Henke et al. 1982). $C_{6.4\mathrm{keV}}$ is the observed Fe I Kα line flux of 2.8×10^{-5} photons cm^{-2} s^{-1}.

We discuss candidates for the irradiating source by estimating its luminosity with equation (1). One is a bright X-ray source, 1E 1743.1−2843, the PSF tail of which is seen at the northwestern edge of the XIS FOV in figure 2. 1E 1743.1−2843 is reported to be a neutron star or a black-hole low-mass X-ray binary in the GC region, or toward the GC region, but beyond there (Porquet et al. 2003; Del Santo et al. 2006).

In the case that 1E 1743.1−2843 is located in the GC region, the projected distance to the M0.51−0.10 XRN is $D = 40$ pc. Since the power-law slope for the X-ray spectrum of 1E 1743.1−2843 is reported to be $\Gamma = 1.9$ by Porquet et al. (2003), we obtained that a luminosity of 2×10^{38} ergs s^{-1} is required for the 6.4 keV line flux of M0.51−0.10. However, 1E 1743.1−2843 persistently has a luminosity of $(1-4) \times 10^{36}$ ergs s^{-1} (e.g., Cremonesi et al. 1999; Porquet et al. 2003), which is 2-orders lower than the required luminosity. In addition, no bursts have been observed from 1E 1743.1−2843 in extensive observations over the last 20 years. In the case that 1E 1743.1−2843 would be beyond the GC region, it is too far to account for the 6.4 keV line flux of M0.51−0.10. Thus, 1E 1743.1−2843 is unlikely to be the irradiating source of M0.51−0.10.

The total luminosity of all cataloged bright point sources within 50 pc (20′) from M0.51−0.10 is $\sim 3 \times 10^{35}$ ergs s^{-1}, which is far lower than the required luminosity of 10^{38-39} ergs s^{-1}.

Koyama et al. (1996), Murakami et al. (2000), and Murakami et al. (2001b) have proposed a GC supermassive black hole, Sgr A*, as the irradiating source of other X-ray reflection nebulae, Sgr B2 and Sgr C. Sgr A* is then thought to have been $\sim 10^6$ times brighter about 300 years ago, the light traveling time between Sgr B2 and Sgr A*.

We applied the XRN scenario by past activity of Sgr A* to M0.51−0.10. The Sgr B molecular complex, consisting of Sgr B1 ($l \sim 0.^\circ5$) and B2 ($l \sim 0.^\circ8$), belongs to the "Galactic-Center molecular Arm" surrounding Sgr A* (Sofue 1995). Sgr B1 and Sgr B2 are located at the same three-dimensional distance from Sgr A* (~ 100 pc) though the projected distances are different. The photon index for Sgr A* is reported to be $\Gamma = 2.7$ by Baganoff et al. (2003), which is not consistent with that of M0.51−0.10 ($\Gamma = 1.3 - 2.2$). However, Baganoff et al. (2001) reported that the photon index became hard ($\Gamma \sim 1.0$) when Sgr A* was in a flare-up state. Koyama et al. (1996) and Murakami et al. (2000) assumed that the photon index is 2.0 for the power-law spectrum of Sgr A*, and reported that the required luminosity for Sgr B2 XRN is $\sim 3 \times 10^{39}$ ergs s^{-1}. With the same assumption, we estimated the required luminosity for M0.51−0.10 to be $\sim 2 \times 10^{39}$ ergs s^{-1}. Thus, it is consistent with the required luminosity for Sgr B2. Therefore, the XRN scenario by the past activity of Sgr A*, which was successfully applied to Sgr B2, may also be applied to M0.51−0.10. Taking into account that Sgr B1 and Sgr B2 have the same three-dimensional distance from Sgr A*, we presume that both of the two XRNe originated in the identical past activity of Sgr A* about 300 years ago.

5. Summary

With Suzaku, we observed of the Sgr B1 region with an exposure time of about 100 ksec in March 2006. Thanks to the excellent energy resolution of the XIS aboard Suzaku, the large effective area and a long exposure, we successfully revealed the distribution of the GCDX, and discovered a new diffuse faint source, "G0.42−0.04", and obtained an excellent spectrum from the 6.4 keV cloud, "M0.51−0.10".

- The line-flux ratio [Fe XXVI]/[Fe XXV] of the Sgr B1 and B2 regions ($l = +0.^\circ3 - -+0.^\circ8$) is consistent with that of the region at $l = -0.^\circ4 - -+0.^\circ2$. The Fe XXV line flux exponentially decreases from the GC center to the Sgr B1 and B2 regions. This result suggests that the GCDX extends at least up to the Sgr B1 and B2 regions with a constant temperature of $kT \sim 6 - 7$ keV.

Table 4. Comparison between required luminosities and observed luminosities.

Irradiating source candidates	Distance* D (pc)	Photon index Γ	$L_{\rm obs}{}^{\dagger}$ (ergs s^{-1})	$L_{\rm req}{}^{\S}$ (ergs s^{-1})
1E 1743.1−2843	40	1.9†	3×10^{36}	2×10^{38}
Sgr A*	100	2.0‡	2×10^{33}	2×10^{39}

Those source are assumed to be at the same distance as M0.51−0.10, 8.5 kpc. The bright source 1E 1743.1−2843 is a neutron star or black hole LMXB. Sgr A* is a supermassive black hole at the center of our galaxy.
* Distance to M0.51−0.10.
† Observed photon index and luminosity (Porquet et al. 2003; Baganoff et al. 2003).
‡ Assumed value by Koyama et al. (1996) and Murakami et al. (2000).
§ Required luminosity to account for the observed 6.4 keV flux of M0.51−0.10. It is obtained from equation (1).

- The large absorption column of $N_{\rm H}\sim8\times10^{22}$ cm^{-2} toward G0.42−0.04 suggests that the source is located in the GC region. The spectra of G0.42−0.04 are well fitted with a thin thermal-plasma model of $kT\sim0.7$ keV. In consideration of the large absorption column toward the GC region, the observational results are consistent with the idea that G0.42−0.04 might be a part of an SNR. On the other hand, G0.42−0.04 is unlikely to be a stellar cluster, since no infrared stellar cluster has been reported at the position of G0.42−0.04.
- M0.51−0.10 is identified with the 6.4 keV cloud "Sgr B1" detected by Yusef-Zadeh et al. (2007). The X-ray spectra of M0.51−0.10 exhibit a absorption column of $N_{\rm H}\sim1.5\times10^{23}$ cm^{-2} and a large equivalent width of ~1.4 keV for the Fe I Kα fluorescence emission line. This suggests that the 6.4 keV X-ray emission is unlikely to be due to the collision of low-energy cosmic-ray electrons, but due to the reflection of external hard X-rays, and hence M0.51−0.10 is thought to be an X-ray reflection nebula. The bright X-ray point source 1E 1743.1−2843, or the collection of fainter point sources near M0.51−0.10 does not explain the luminosity of $\gtrsim10^{38-39}$ergs s^{-1} required for the 6.4 keV X-rays from M0.51−0.10. The XRN scenario based on the past activity of Sgr A*, which was successfully applied to Sgr B2, may also be applied to M0.51−0.10.

We are grateful to all members of the Suzaku hardware and software teams and the science working group. HN, TI and YH are supported by Japan Society for the Promotion of Science (JSPS) Research Fellowship for Young Scientists. This work is based by a Grant-in-Aid for the 21st Century COE "Center for Diversity and Universality in Physics" from Ministry of Education, Culture, Sports, Science and Technology (MEXT) of Japan, and is supported by a Grant-in-Aid for Scientific Research on Priority Areas in Japan (Fiscal Year 2002-2006); "New Development in Black Hole Astronomy". This work is also partially supported by Grants-in-Aid for Scientific Research of JSPS Nos. 18204015, 18540228, 18740105.

References

Baganoff, F. K., et al. 2001, Nature, 413, 45
Baganoff, F. K., et al. 2003, ApJ, 591, 891
Cremonesi, D. I., Mereghetti, S., Sidoli, L., & Israel, G. L. 1999, A&A, 345, 826
Del Santo, M., Sidoli, L., Bazzano, A., Cocchi, M., De Cesare, G., Paizis, A., & Ubertini, P. 2006, A&A, 456, 1105
Dutra, C.M., & Bica, E. 2000, A&A, 359, L9
Henke, B. L., Lee, P., Tanaka, T. J., Shimabukuro, R. L., & Fujikawa, B. K. 1982, At. Data Nucl. Data Tables, 27, 1
Hyodo, Y., Tsujimoto, M., & Koyama, K. 2008, PASJ, 60, (#3169)
Ishisaki, Y., et al. 2007, PASJ, 59, S113
Kokubun, M., et al. 2007, PASJ, 59, S53
Koyama, K., Awaki, H., Kunieda, H., Takano, S., Tawara, Y., Yamauchi, S., Hatsukade, I., & Nagase, F. 1989, Nature, 339, 603
Koyama, K., Maeda, Y., Sonobe, T., Takeshima, T., Tanaka, Y., & Yamauchi, S. 1996, PASJ, 48, 249
Koyama, K., Hyodo, Y., & Inui, T. 2006, Journal of Physics Conference Series, 54, 95
Koyama, K., et al. 2007a, PASJ, 59, S23
Koyama, K., et al. 2007b, PASJ, 59, S221
Koyama, K., et al. 2007c, PASJ, 59, S245
Law, C., & Yusef-Zadeh, F. 2004, ApJ, 611, 858
Mehringer, D. M., Palmer, P., & Goss, W. M. 1993, ApJ, 402L, 69M
Mitsuda, K., et al. 2007, PASJ, 59, S1
Mori, H., Tsuru, T. G., Hyodo, Y., Senda, A., & Koyama, K. 2008, PASJ, 60, (#3131)
Muno, M. P., et al. 2004, ApJ, 613, 326
Muno, M. P., Bauer, F. E., Bandyopadhyay, R. M., & Wang, Q. D. 2006, ApJS, 165, 173
Murakami, H., Koyama, K., Sakano, M., Tsujimoto, M., & Maeda, Y. 2000, ApJ, 534, 283
Murakami, H., Koyama, K., & Maeda, Y. 2001, ApJ, 558, 687
Murakami, H., Koyama, M., Tsujimoto, M., Maeda, Y., & Sakano, M. 2001, ApJ, 550, 297
Porquet, D., Rodrigues, J., Corbel, S., Goldoni, P., Warwick, R. S., Goldwurm, A., & Decourchelle, A. 2003, A&A, 406, 299
Revnivtsev, M., Vikhlinin, A., & Sazonov, S. 2006, astro-ph/0611952
Serlemitsos, P. J., et al. 2007, PASJ, 59, S9
Sofue, Y. 1990, PASJ, 42, 827
Sofue, Y. 1995, PASJ, 47, 527

Takahashi, T., et al. 2007, PASJ, 59, S35
Tatischeff, V. 2003, in Final Stage of Stellar Evolution, ed. C. Motch & Hameury (EAS publication Series vol.7), 79 (astro-ph/0208397v1)
Tsujimoto, M., Hyodo, Y., & Koyama, K. 2007, PASJ, 59, S229
Yamauchi, S., Kawada, M., Koyama, K., Kunieda, H., Tawara, Y., & Hatsukade, I. 1990, ApJ, 365, 532
Yusef-Zadeh, F., Muno, M., Wardle, M. 2007, & Lis, D. C. 2007, ApJ, 656, 847